GEOLOGIA • 2011 • Tom 37 • Zeszyt 4 • 481–501

APPLICATION OF SIMPLE SEISMIC MODELS FOR INTERPRETATION OF SMALL REEF OBJECTS UNDER CONDITIONS OF LOW RESOLUTION SEISMIC DATA AND INCOMPLETE BOREHOLE INFORMATION

Wykorzystanie prostych modelowań sejsmicznych do interpretacji małych obiektów rafowych w przypadku niskorozdzielczych danych sejsmicznych i ubogich danych otworowych

Jan BARMUTA & Kaja PIETSCH

AGH University of Science and Technology, Faculty of Geology, Geophysics and Environmental Protection, Department of Geophysics; al. Mickeiwicza 30, 30-059 Kraków, Poland; e-mail: jbarmuta@geol.agh.edu.pl, pietsch@agh.edu.pl

Abstract: Tracing facies and saturation with hydrocarbon along sedimentary beds is one of Seismic's most important objectives. The application of simple seismic modeling for the interpretation of low resolution seismic data is presented. This method confirmed the possibility to trace changes in Main Dolomite (Ca2) development and to detect, comparatively small to the seismic resolution, hydrocarbon traps.

Key words: seismic interpretation, seismic modeling, Main Dolomite (Ca2), reef structures

Treść: Śledzenie zmian w wykształceniu facjalnym oraz nasycenia węglowodorami jest jednym z najważniejszych zadań postawionych sejsmice. W artykule przedstawiono sposób wykorzystania prostych modelowań sejsmicznych w interpretacji niskorozdzielczych danych sejsmicznych. Potwierdzono również możliwość śledzenia zmian w wykształceniu dolomitu głównego (Ca2) oraz wykrywania niewielkich, w stosunku do rozdzielczości sejsmiki, nagromadzeń węglowodorów.

Słowa kluczowe: interpretacja sejsmiczna, modelowanie sejsmiczne, dolomit główny (Ca2), struktury rafowe

INTRODUCTION

Seismic data older than several decades or even data which is only a decade and a few years is hard to interpret because it was obtained by less advanced methods of acquisition and processing.

Seismic profiles from those years are typically of a much lower vertical and horizontal resolution. Additionaly, these less advanced methods did not allow for the generation of the type of high quality seismic sections which are available nowadays.

The purpose of this research is to show the potential of basic seismic modeling applied to interpretation of structural objects or reservoirs of a size close to the seismic resolution, which has low quality seismic data, scarce geophysical borehole logs and incomplete geological information.

Presented are the results of attempted detailed structural interpretation of small reef objects within sediments of Main Dolomite (Ca2) of Stassfurt cyclothem (Z2). Another objective was the identification of locations potentially yielding hydrocarbons. The analyzed objects are situated within the carbonate platform between Zielona Góra and Nowa Sól – the area in which accumulations of oil and gas have already been confirmed (Karnkowski 2007b). The expected reef structures are probably of small size, hence the resolution of seismic record becomes critical, since it determines the detection limits. Seismic sections used for the purpose of this paper were of poor quality. This could be a consequence of less advanced seismic acquisition and processing techniques which were available in the nineteen eighties as well as complex geology of thin-layered sediments of Zechstein. Non-standard methods of interpretation became necessary in this situation.

For this particular case, interpretation of facies and reservoirs was accomplished by simple, multi-optional seismic modeling carried out using the GeoGraphix computer program from Landmark Graphics Corp.

GEOLOGICAL CHARACTERISTICS OF THE RESEARCH AREA

The investigated area is a part of Fore-Sudetic Homocline on the depression of Zielona Gora demarcated from North by Wolsztyn High and from the South by Fore-Sudetic Block (Stupnicka 1997). Within the analyzed area, the sediments of Fore-Sudetic Homocline rest directly on the clastic deposits of younger Upper Carboniferous belonging to Variscan structural division (Borehole documentation). Permian sediments encountered in oil and gas exploratory boreholes were identified as Lower Permian – Rotliegendes and to Upper Permian – Zechstain. Volcanic rocks as well as clastic sediments of Saxon formed during the Rotliegendes period (P1). In the Upper Permian, cyclical sediments typical for marine evaporation were formed as a result of Zechstein sea transgressions.

The cyclothems have various thicknesses and consist of beds of salt, anhydrite, limestone, dolomite, marl and claystone. Numerous structures like diapirs, salt domes, pillows or ridges can be observed within the beds (Wagner 1994). The barrier reefs identified in the two oldest cyclothems Werra (PZ1) and Stassfurt (PZ2) were confirmed to be often accumulating hydrocarbons (Karnkowski 2007a, 2007b).

The distribution of facies within prospective layers of PZ1 and PZ2 cyclothems reflects the paleogeographical variations (Fig. 1). The Triassic formation, that directly overlays the Permian deposits, can be divided into three areas. In the South area the Lower Triassic developed mainly as Bunter Sandstone – monotonous profile of intercalating claystones, mudstones, sandstones and limestones. The Middle Triassic is represented by Muschelkalk consisting of limestone and dolomite with anhydrite and claystone inserts. While in the North part, Triassic formation can be found as terrigenous sediments of Keuper. The total thickness of Triassic formation often exceeds 1000 m.

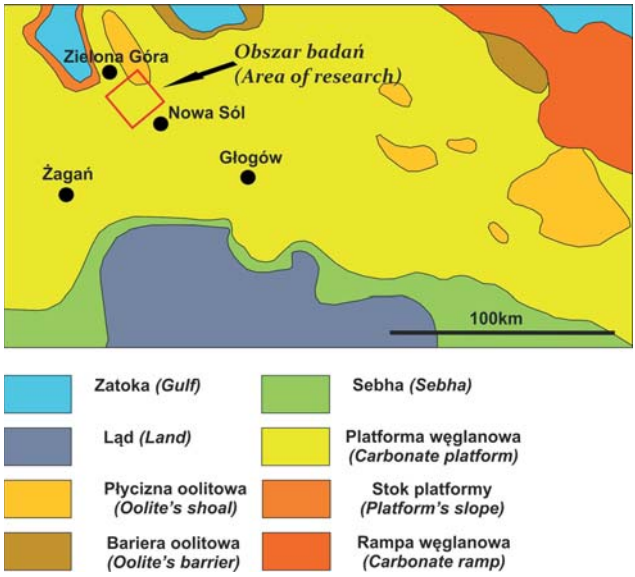

Fig. 1. Research area location on paleogeographic map section (Kotarba et al. 2009, changed)

Fig. 1. Lokalizacja terenu badań na fragmencie mapy paleogeograficznej (Kotarba *et al.* 2009, zmienione)

The Cimmerian and in particular the Laramian phase of the Alpine orogeny, led to the development of two major sets of faults of NW-SE and NNE-SSE direction, and thus dividing the Fore-Sudetic Homocline into blocks (Urabński 1998, Sztormwasser 1999).

Characteristics of Main Dolomite

From an oil and gas exploration point of view, of significance are Poland's Permian basin formations which are sediments of numerous transgressions and regressions of the Permian sea (Fig. 1). In particular, Permian's Rotliegendes and carbonate formations of Zechstein are a prospect for accumulations of hydrocarbons (Niedbalec & Radecki 2007, Karnkowski 2007a, 2007b). The Main Dolomite (Ca2) of Zechstain basin is recognized as a major

reservoir-bearing strata, from which the Stassfurt cyclotheme (PZ2) begins. Main Dolomite carbonate beds formation was predominantly affected by morphology of the sea bed shaped by the earlier cyclothem Werra (PZ1) (Wagner 1994) (Fig. 2). Limestone and dolomite are typical sediments of Main Dolomite (Ca2). Barrier reefs were formed mainly on carbonate platforms that were encircling the abyssal planes. Microplatforms can also be found within abyssal plane areas (Wagner 1994, Karnkowski 2007b).

The porosity of these rocks is attributed to jointing and caverns that are commonly filled with carbonate and sulphate cements. The type and magnitude of Main Dolomite porosity varies largely and depends mainly on facies and diagenesis. It can reach more than 20% and is usually higher in granular facies than mud facies (Pikulski 1996).

However, even at high porosity, hydraulic conductivity of Main Dolomite rocks is typically low or close to zero. The Main Dolomite profile within the barrier zone shows three distinctly characteristic sections (information significant for the further research) (Protas 1997). The section closer to the bottom comprises of transitional dolomite characterized by a high content of clay and anhydrite. The middle section consists of dolomite, which display variability typical for high energy sediments. It is represented mainly by onkoid-intraclast grainstones and onkoid-intraclasts grainstones with algean laminoids. The upper section, which is also dolomite of high energy environment, is developed as onkoid-intraclast grainstones. The best conditions for reservoir formation are most often observed in the middle section (Pikulski 1996). Geochemical investigation shows that Main Dolomite can be a source rock as well as a reservoir rock for hydrocarbons. Facies related to deep sea and fore-barrier zone are thought to have the potential of generating hydrocarbons (Pikulski 1996).

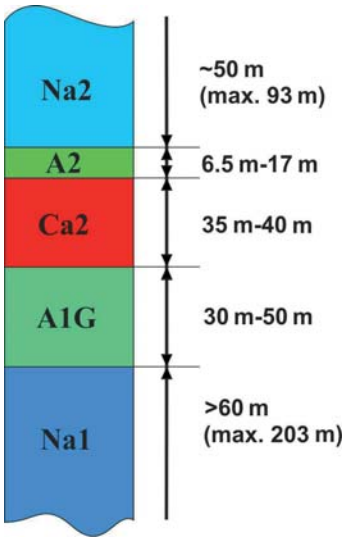

Fig. 2. Synthetic lithologic profile of cyclothems Werra and Stassfurt

Fig. 2. Syntetyczny profil litologiczny warstw cyklotemu Werra i Stassfurt

In the investigated area the Main Dolomite overlays 30–50 m thick Upper Anhydrite (A1G) below which an Oldest Halite (Na1) bed is observed in the profile (usually 60 m and locally reaching 200 m thickness) (Fig. 2). The average thickness of Main Dolomite in exploratory boreholes is 35 m and locally 40 m. It needs to be noted that the exploratory boreholes were most often located within reef buildups, so in a lagoon or in a deep water zone this thickness could be much smaller. Basal Anhydrite (A2) of a thickness varying from 6.5 m to 17 m rests on the carbonate deposits of Main Dolomite. The thickness of A2 decreases towards the North and can be found to be more than 10 m thick only on the South margin of the investigated area. Anhydrites beds are impervious therefore, they prevent to a high degree the migration of hydrocarbons to the overlying strata. From a seismic point of view and based on the thickness range presented in figure 2, A2 and Ca2 beds can be categorized as a thin-layered configuration. Older Halite (Na2) with a maximum thickness of 93 m and a commonly encountered thickness of 50 m (borehole documentation) is present above A2 in the profile.

DATA AND METHODS

The research area is covered by 22 seismic profiles. The seismic survey was carried out in the years 1982–1984 by Geofizyka Toruń Sp. z o.o. as a part of the larger 2D Nowa Sól – Wschowa scheme (Figs 1, 3).

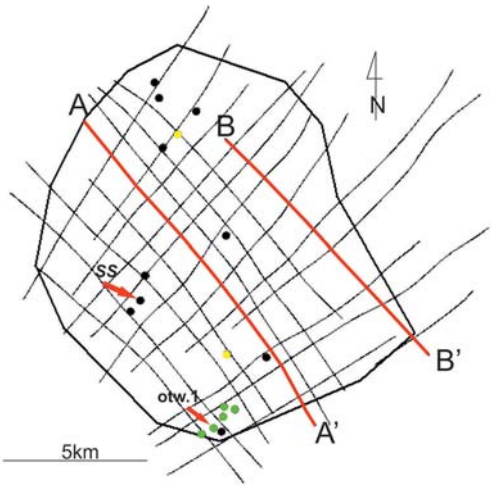

Fig. 3 Location of seismic profiles and boreholes within research area. Yellow inicates boreholes with sonic logs, green – boreholes with logs of average velocity; SS – borehole with synthetic seismogram, otw.1 – borehole encountering hydrocarbon accumulation, A-A', B-B' sections analyzed in the paper

Fig. 3. Mapa przekrojów sejsmicznych oraz otworów na badanym terenie. Na żółto zaznaczono otwory, dla których dostępne było profilowanie akustyczne, na zielono – profilowanie prędkości średnich; SS – otwór z zaprezentowanym sejsmogramem syntetycznym, otw.1 – otwór nawiercający złoże, A-A', B-B' – profile analizowane w artykule

Additionally, two logs of average velocities as well as geophysical logs from eighteen boreholes irregularly distributed over the investigated area (Fig. 3) were also available to the authors. The majority of these boreholes and geophysical logging were carried out in the nineteen-sixties and seventies. The geophysical investigation in boreholes was mostly limited to various types of electrometric and natural gamma radiation (GR) profiling. In several cases the GR records were provided in non-standard units i.e. the count of impulses over time. There was no availability of interpretation profiles e.g. porosity curve, density curve or saturation curve. However, full lithostratigraphic logs of all boreholes were provided and in some cases for select intervals results of laboratory petrophysical tests – mainly porosity, hydraulic conductivity and saturation.

Interval transient time (DT) profiling was carried out in only five boreholes located at the South periphery of the investigated area (Fig. 3).

APPLIED METHODS

A multi-stage algorithm was developed for the purpose of data analysis.

In the first stage the borehole geophysics data were processed to obtain interval transient time curves (DT). This information allowed for reliable correlation of seismic horizons to geological boundaries by the use of synthetic seismograms. The second stage covered geological interpretation of the seismic data. The phase correlation of seismic horizons and multi-optional seismic modeling, on which the interpretational criteria were developed along with the resulting reservoir-wise interpretation of registered wave field, were carried out in subsequent steps.

Determination of transient time curves

When interpreting the available seismic data it became apparent that the major difficulty is the lack of records for the interval transient time (DT). This parameter was recorded in only 5 boreholes located at the perimeter of the investigated area (Fig. 3), for which the seismic record was particularly disturbed, to a level preventing confident correlation between the seismic and borehole data. In light of this situation, for the purpose of enhancing the reliability of the interpretation, the transient times were determined indirectly (Barmuta 2010). The method used is based on identifying the dependency between transient time (DT) and natural gamma radiation (GR) in boreholes for which both parameters were recorded. The dependencies were described for every lithostratigraphic interval identified in boreholes, such as: Main Dolomite (Ca2), Basal Anhydrite (A2), Older Halite (Na2), Roof Anhydrite (A2G), Main Anhydrite (A3), Younger Halite (Na3) and Youngest Halite (Na4). The Mesozoic Bunter Sandstone as well as a Cenozoic cover were considered as one interval. An example of cross-plot DT vs. GR created for Main Dolomite (Fig. 4) and Basal Anhydrite (Fig. 5) illustrate the method of determining the dependency. The obtained dependency of transient time (DT) on natural gamma radiation (GR) was used to calculate the transient time (DT) in the remaining boreholes where natural gamma radiation (GR) logs were available. Reliability of the method was tested by the determination of a synthetic transient time

(DT) curve for the borehole at which this parameter was recorded (Fig. 6). Comparison of the synthetic and logged DT curves, generally demonstrates good conformity within Zechstein beds. However, it appears that the synthetic DT curve within Triassic and Tertiary strata only shows a general trend which does not allow linking the borehole and seismic horizons within this depth interval.

Despite the good test results within Zechstein strata, it needs to be understood that the synthetic transient time curve may not always represent actual variations of this parameter within the rocks. It may, for example, mirror variable properties of the Main Dolomite related to zones of deposition, or degree of saturation with hydrocarbons.

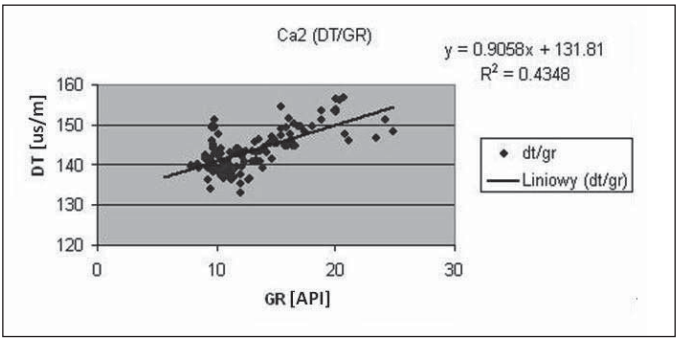

Fig. 4. Cross-plot of interval transient time (DT) vs. natural gamma radiation (GR) for Main Dolomite (Ca2)

Fig. 4. Wykres krzyżowy czasu interwałowego (DT) i promieniowania naturalnego gamma (GR) dla dolomitu głównego (Ca2)

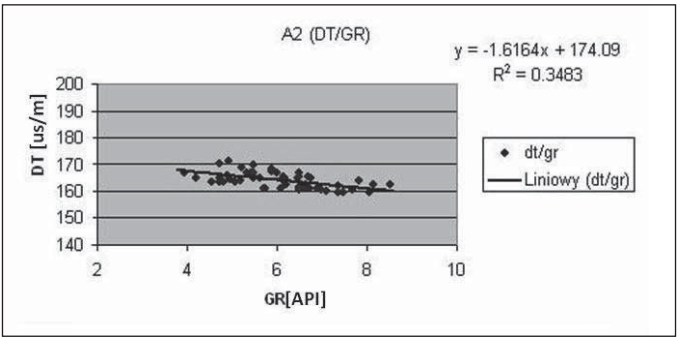

Fig. 5. Cross-plot of interval transient time (DT) vs. natural gamma radiation (GR) for Basal Anhydrite (A2)

Fig. 5. Wykres krzyżowy czasu interwałowego (DT) i promieniowania naturalnego gamma (GR) dla dolomitu dla anhydrytu podstawowego (A2)

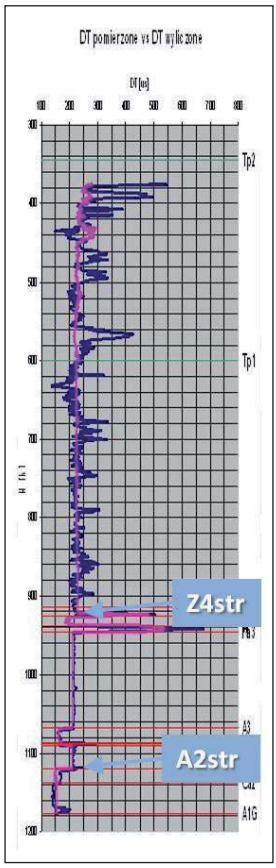

Fig. 6. Juxtaposition of synthetic DT curve (pink) and logged DT curve (dark blue)

Fig. 6. Porównanie wyliczonej krzywej DT (krzywa różowa) z krzywą pomierzoną (krzywa granatowa)

Seismic vertical resolution and tuning thickness

Thin layered rock-mass and poor quality seismic records necessitate detailed analysis of seismic data resolution (Fig. 2). Seismic resolution can be determined based on velocity of propagating wave and frequency characteristics of the recorded seismic signals.

The wave velocity in Main Dolomite depends mainly on facies and saturation. Based on borehole data it was determined that the wave velocity for compacted unsaturated dolomite was 6500 m/s, while for porous and saturated it may drop as low as 3500 m/s.

The predominant frequency of the signal extracted from the available seismic traces was determined to be 30 Hz. It should be taken into consideration that the program used for extraction of the signal calculates the frequency and amplitude spectra from the starting point of the seismic trace where high frequencies, further fading with depth, are still present. Be-

cause of this effect on the depth of Zechstein strata, the spectrum of the signal can be shifted towards lower frequency values. This was confirmed by synthetic seismograms which show that a 26 Hz signal best fits the recorded seismic section (Fig. 7).

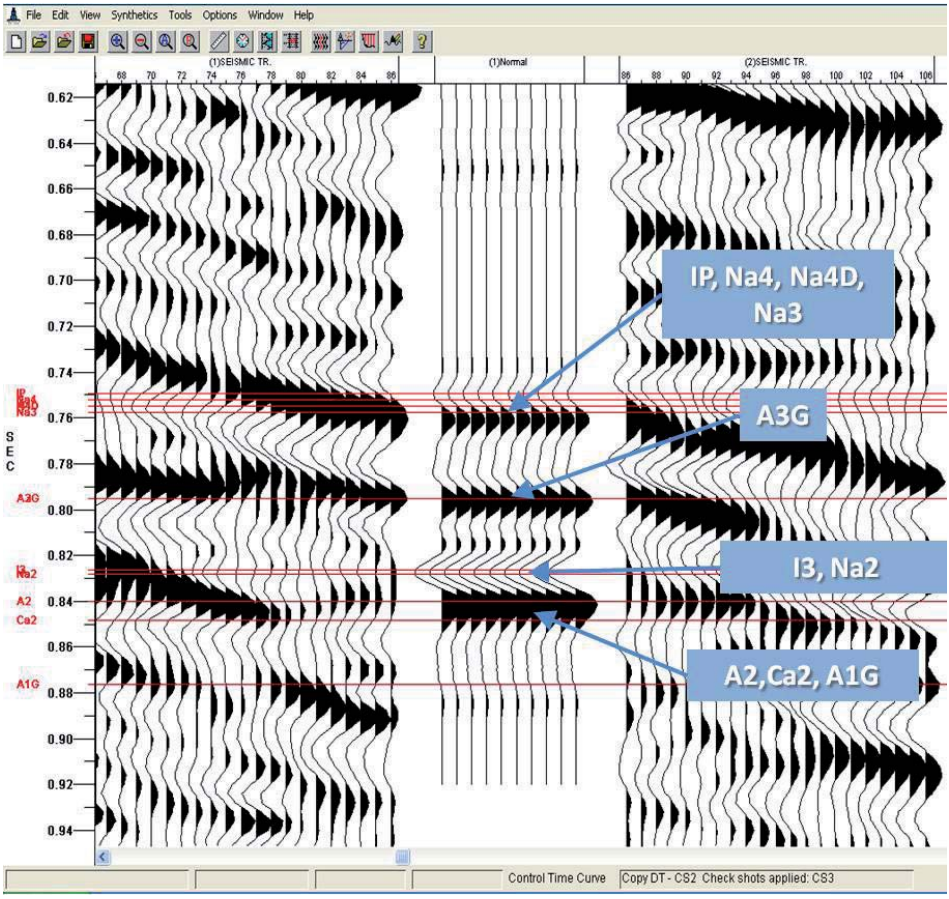

Fig. 7. Synthetic seismogram generated from synthetic DT curve and Ricker's signal 26 Hz

Fig. 7. Sejsmogram syntetyczny wygenerowany na podstawie wyliczonej krzywej DT oraz sygnału Rickera 26 Hz

Widess criterion (Widess 1973), which states that the maximum amplification of the reflected signal amplitude (tuning) occurs when the bed thickness $h = 1/4\lambda$ (where λ is the wave length) was used for the evaluation of seismic resolution. In the case of thicker beds the signals reflected from the bottom and the ceiling of the bed can be differentiated, while in the case of layers thinner than $1/8\lambda$ the interfered signal becomes practically identical with single reflection from the ceiling. Because of the generally low quality of the seismic data, the minimum detectable thickness of a single layer was assumed as $1/4\lambda$.

By applying Widess's criterion it was possible to determine the critical thicknesses of Main Dolomite, detectable when assuming a predominant frequency of 26 Hz and variable wave velocity. At the extreme wave velocities i.e.: 6500 m/s and 3500 m/s the tuning thickness becomes 62.5 m and 33.5 m respectively. Yet it should be highlighted, that as borehole geophysics show, the Main Dolomite bed is not thicker than 50 m within the barrier. Hence, it can be presumed that in other zones, such as deep water and lagoon, its thickness is much smaller. The next layer that is significant for further deliberation is Basal Anhydrite (A2), which has a varying thickness generally close to 10 m with the exception of a recorded value of 20 m in only one borehole. At a wave velocity of 6000 m/s the tuning thickness is 60 m. Because of this value the reflection signals from the ceilings of Basal Anhydrite and Main Dolomite cannot be separated and are consequently detected as one signal. In the case where both reflexes are positive the resulting reflex should be positive and strong. Such an effect can be expected at locations where Main Dolomite is compacted and unsaturated. A decrease of wave amplitude can be anticipated in an opposite situation i.e. when the wave velocity in Main Dolomite is smaller than in Basal Anhydrite. This effect may correspond to a condition of porous and saturated Ca2 layer. Amplitude variations of the signal reflected from A2 ceiling are a subject which is analyzed in a further section of this paper. Interference of reflected signals from the ceilings of three layers: Basal Anhydrite (A2), Main Dolomite (Ca2) and Upper Anhydrite (A1G) is possible in the case when the thickness of Ca2 is smaller than tuning thickness.

Geological interpretation of seismic data

Curves of synthetic transient time (DT), calibrated against average velocities and extracted seismic signal, were used to construct synthetic seismograms using the Well Editor in the GeoGraphix program from Landmark Graphics Corp. The resultant seismograms were the basis for further correlating seismic horizons and geological features.

The presented seismogram in (Fig. 7) clearly shows the interfered reflex from Basal Anhydrite (A2) and from Main Dolomite (Ca2). In addition, a reflex from Main Dolomite's (A3) ceiling can also be identified. The other remaining boundaries are hard to determine due to a low frequency signal, lack of density logs (necessary for calculation of acoustic impedance), as well as errors in determining the synthetic DT curve. The lack of measured DT within sediments below Main Dolomite precluded linking Upper Anhydrite (A1G) and Oldest Halite (Na1) with seismic horizons. Structural interpretation performed on recorded seismic sections revealed the general features of Zechstein formations including among others: location of salt structures, localized paleo-heaves, and reef barrier zones towards which hydrocarbon exploration could be directed. The salt structures within Oldest Halite (Na1) which were interpreted on seismic sections are characteristic ridges and salt pillows (e.g. profile B-B' – Figs 3, 8). Discontinuities of seismic horizons that can be visible within salt structures are likely, among possible causes, a result of an erroneously performed migration procedure. Most importantly, reef buildups were confirmed on several sections despite the identification being obscured by the seismic data's poor quality. The sizes of most reef structures are close to the seismic resolution or just slightly bigger, hence their typical signatures (Jędrzejowska-Tyczkowska *et al.* 1997) cannot be found or are hardly discernable.

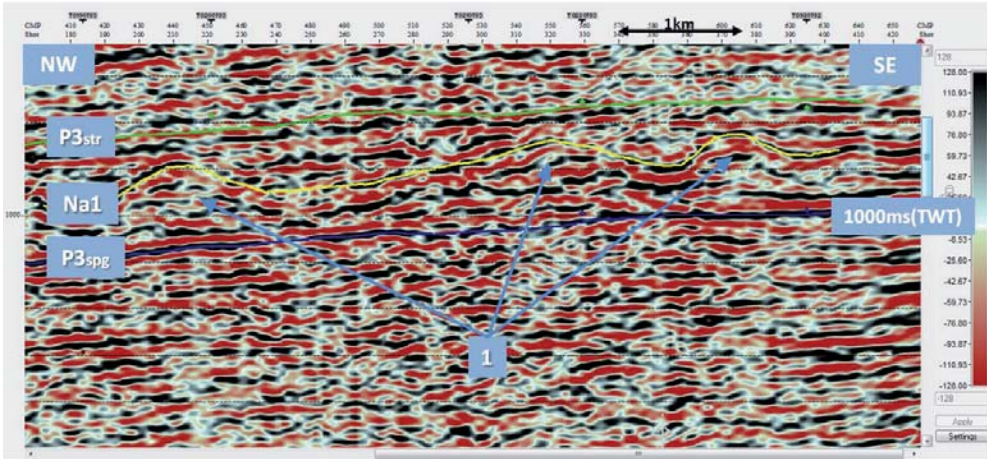

Fig. 8. Salt pillows (1) within Oldest Halite beds (Na1) on section B-B': Na1 – Oldest Halite, P3 – bottom of Zechstein, P3 – ceiling of Zechstein

Fig. 8. Poduszki solne (1) w utworach soli najstarszej Na1 na profilu B-B': Na1 – sól najstarsza, P3spg – spąg cechsztynu, P3str – strop cechsztynu

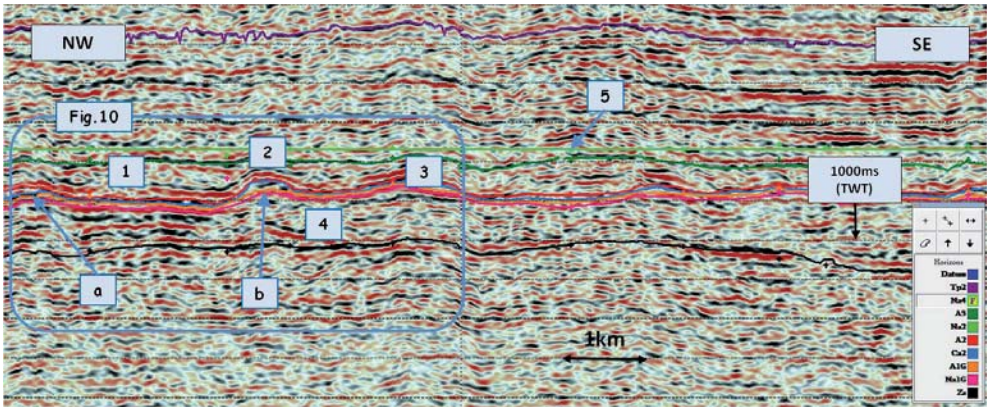

Fig. 9. Section A-A' with complete barrier zone. 1 – deep sea zone, 2 – main barrier zone, 3 – lagoon zone, 4 – paleoheave, 5 – flattened horizon, a, b – analyzed objects (Fig. 10)

Fig. 9. Profil A-A' przedstawiający w pełni wykształconą strefę barierową: 1 – strefa głębokomorska, 2 – strefa bariery właściwej, 3 – strefa lagunowa, 4 – paleopodniesienie, 5 – „wypłaszczony" horyzont, a, b – obiekty analizowane w artykule (Fig. 10)

An example of a seismic record clearly depicting a reef barrier is seismic section A-A' (Fig. 9), it distinctly shows all the features of carbonate reef buildup. For better contouring

of this particular structure, a procedure of flattering was applied to Youngest Halite (Na4) horizon. Three zones become evident within Main Dolomite as a result of this adjustment in the seismic record. These paleo-environmental zones can be identified on profile A-A': deep sea zone (1), the main barrier (2) and lagoon zone (3) further to the South-East (Barmuta 2010).

Moreover, the paleo-heave mirroring the shape of underlying sediments of cyclothem Werra (4) that created the favorable condition for reef development and reef sedimentation are clearly depicted. From a hydrocarbon prospecting point of view other interesting objects are as follows: a small object "a" at the peripheral part of the seismic profile A-A' and an area at the crown of the main barrier (object "b") (Figs 9, 10). These elements are further discussed in the next part of this paper.

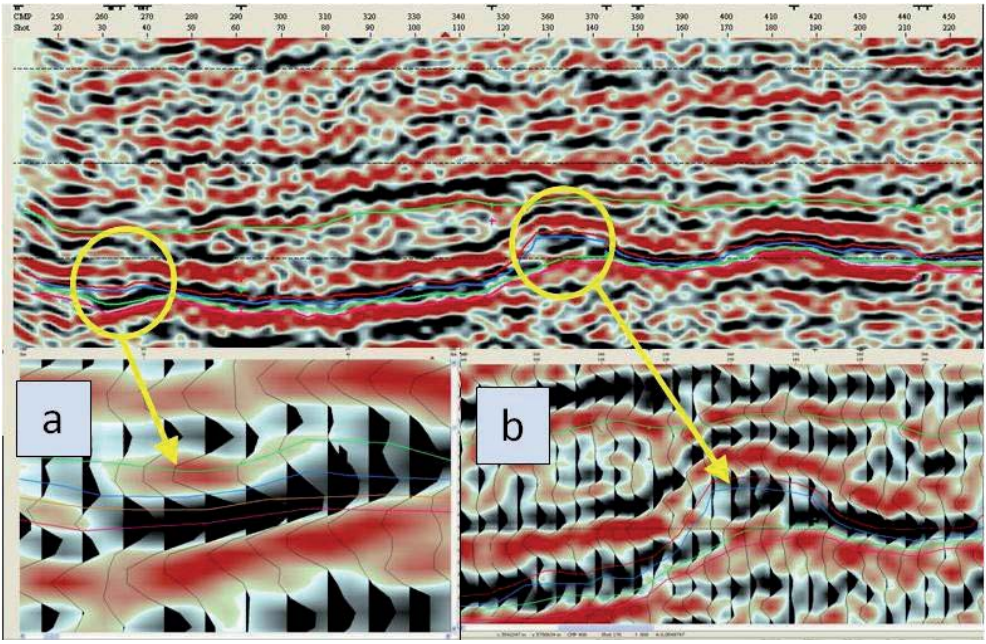

Fig. 10. NW part of A-A' section: a, b – analyzed objects

Fig. 10. NW fragment profilu A-A': a, b – obiekty analizowane w artykule

The poor quality of the seismic records and small dimensions, of reef buildups characteristic for this part of Zechstein basin in Poland (the dimensions comparable to resolution of seismic data), make the interpretation difficult and the obtained depictions of the objects not fully reliable. In this situation, seismic modeling is the tool effectively helping the interpretation and in particular the evaluation of saturation of carbonate buildups.

Modeling

In principle multi-optional seismic modeling compares theoretical seismic wave fields generated for various seismogeological models with the fields actually recorded.

Conformity of theoretical and recorded fields allows for an assumption that the seismogelogical model generating the theoretical field represents the actual rock-mass structures and condition well. Of particular interest are: unusual record appearing on NW part of profile A-A (Fig. 9) within Main Dolomite (Ca2) as well as an arrangement of reflexes within the crown part of the main barrier (object "a" and "b") (Fig. 10). Both locations are potential reservoir zones. They were further interpreted by seismic modeling using the computer program GeoGraphix . Its application Struct. Option *Vertical Incidence* was applied for generating seismic response, assuming verticality of seismic signal (simulation of seismic section after migration) and Ricker's theoretical signal of 26 Hz frequency.

Models I and II were developed to simulate a seismic record of object "a" appearing at the periphery of the profile that likely extends over a deep sea zone. For the purpose of modeling it was assumed that the atypical arrangement of reflexes is related to variations of porosity and saturation of Main Dolomite. Modeling started from calculation of wave field for the deep sea zone of Ca2 at specified constant wave velocities (Model I – Fig. 11).

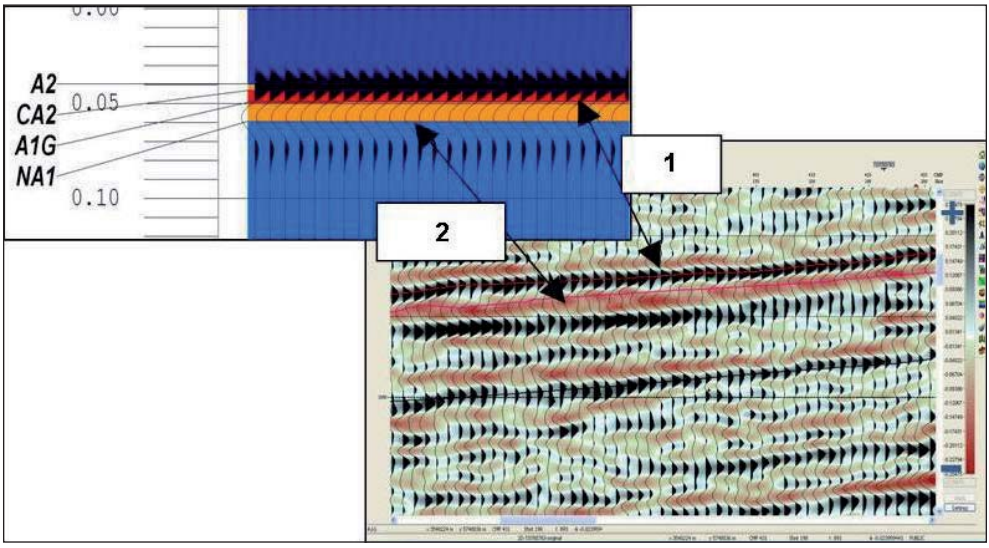

Fig. 11. Juxtaposition of seismic response generated by Model I and actual seismic section. On actual seismic section interfered reflexes are clearly marked (1) from Basal Anhydrite (A2) and Main Dolomite (Ca2) as well as negative reflex (2) at Oldest Halite ceiling (Na1)

Fig. 11. Porównanie wyników modelowań dla Modelu I z profilem sejsmicznym. Na sekcji pomierzonej wyraźnie zaznacza się zinterferowane odbicie (1) od anhydrytu podstawowego (A2) i dolomitu głównego (Ca2) oraz ujemny refleks (2) w stropie soli najstarszej (Na1)

Based on information from bore holes for each of the geological strata in the seismogeological model of this zone the following parameters were assumed:

- Oldest Halite (Na1): P wave velocity – 4800 m/s;
- Upper Anhydrite (A1G): thickness – 30 m, velocity – 6000 m/s;
- Main Dolomite compacted, unsaturated (Ca2): thickness – 20 m, velocity – 6500 m/s;
- Basal Anhydrite (A2): thickness – 10 m, velocity – 6000 m/s;
- Older Halite (Na2): velocity – 4500 m/s.

The theoretical wave field computed from Model I (Fig. 11) shows a clear positive reflex from the ceiling of Basal Anhydrite and a negative reflex from Oldest Halite ceiling.

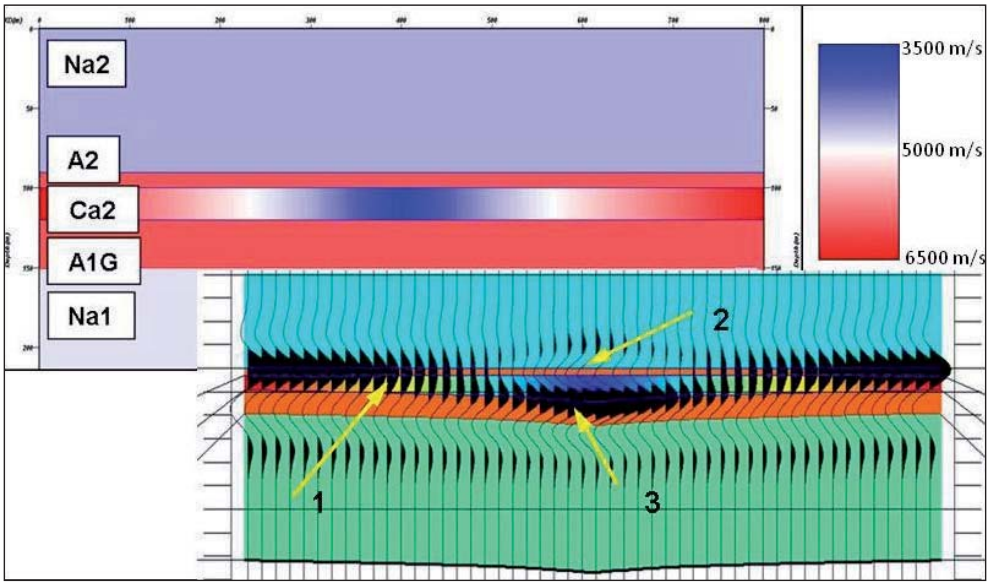

Fig. 12. Model II and its seismic response: 1 – drop of amplitude related to progressive decrease of wave velocity within Main Dolomite (Ca2), 2 – switch of reflex polarization, 3 – time sag and bright spot at the bottom of Main Dolomite (Ca2)

Fig. 12. Model II wraz z odpowiedzią sejsmiczną: 1 – spadek amplitudy związany z postępującym spadkiem prędkości w dolomicie głównym (Ca2), 2 – zmiana polaryzacji refleksu, 3 – ugięcie czasowe (*time sag*) oraz wzrost amplitudy (*bright spot*) w spągu dolomitu głównego (Ca2)

The range of thicknesses and characteristic velocities of layers A2, Ca2, A1G and Na1 indicate that the bed's thickness is close to the resolution of seismic data. It is for this reason that the calculated field shows an interfered wave. The calculated theoretical wave field is in good agreement with the recorded seismic section (Fig. 9 – object 1). Following the initial assumption that the atypical layout of the reflexes in this location, i.e. deep sea zone, is a result of variations of porosity and saturation, the subsequent Model II (Fig. 12) retains the same

thicknesses as Model I, while velocities within Ca2 bed were set to vary horizontally between 6500 m/s to 3500 m/s. On the resultant seismic section the variations of wave velocity produce a characteristic pattern (Fig. 12). Together with a drop of wave velocity from 6500 m/s to about 5000 m/s the amplitude of the reflected wave from A2 ceiling decreases significantly (Fig. 12). A further drop of velocity within Ca2 causes a reflection in A2 ceiling and changes the polarization to negative (Fig. 12). Additionally, within the section of lowest velocities in Main Dolomite, above negative reflection from the Basal Anhydrite ceiling, up to the minute positive reflex may be observed which could be an effect of sideway oscillations related to signal shape. Also, typical indicators of saturated zones DHI become apparent on the profile (i.e. the time sag at the bottom of Ca2 bed in the area of reduced velocities and a distinct bright spot-type rise of wave amplitude – Fig. 12). In summation, the performed modeling allows for the conclusion that this type of layout of reflexes indicates a zone saturated with gas. It can be further inferred with a high probability that the seismic depiction in the NW part of the profile A-A' (Figs 9, 10 – object "a") is a result of a local increase in porosity and saturation of Main Dolomite (Ca2). This conclusion is well substantiated by the presence of all the features in the actual seismic records which were predicted through modeling (Figs 10, 13). It is also confirmed by a seismic image of the hydrocarbon reservoir documented within this area (Fig. 14) Seismic record from this reservoir zone shows a distinct negative reflex and time sag, whereas the area beyond the reservoir zone is contoured by the extent of interfered reflexes from Main Dolomite and Basal Anhydrite like in the theoretical profile (Fig. 12).

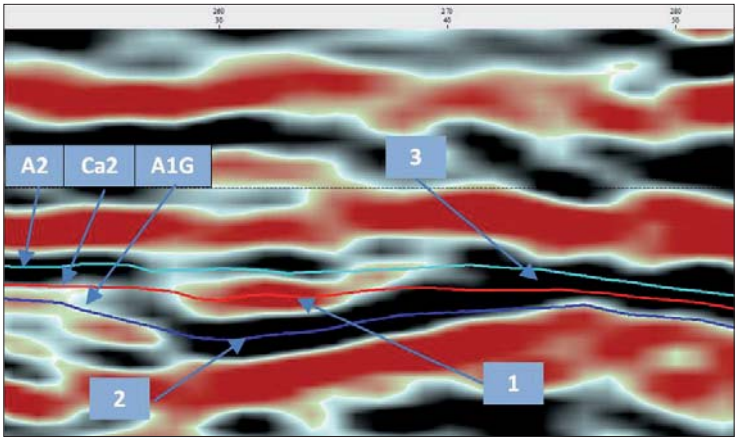

Fig. 13. Seismic record with horizons drawn within object „a" on section A-A': A2 – Basal Anhydrite, A1G – Upper Anhydrite, Ca2 – Main Dolomite, 1 – switch of polarization, 2 – time sag and bright spot (amplitude increase) at the bottom of Main Dolomite, 3 – drop of reflected wave amplitude within area of minor velocity variations within Main Dolomite

Fig. 13. Zapis sejsmiczny z wyrysowanymi horyzontami w obrębie obiektu „a" na profilu A-A': A2 – anhydryt podstawowy, A1G – anhydryt górny, Ca2 – dolomit główny, 1 – zmiana polaryzacji, 2 – ugięcie czasowe spągu dolomitu głównego (*time sag*) oraz wzrost amplitudy (*bright spot*), 3 – spadek amplitudy odbicia w rejonie niewielkich zmian prędkości w dolomicie głównym

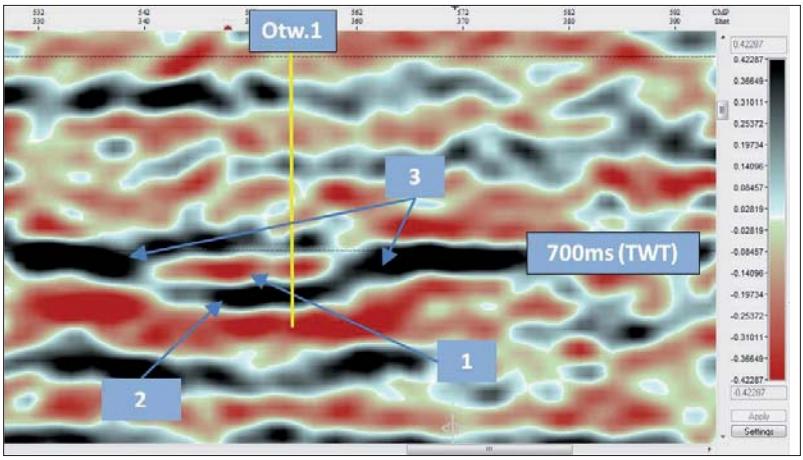

Fig. 14. Documented gas reservoir: 1 – polariazation change within the region around the reservoir, 2 – time sag at the bottom of Main Dolomite (Ca2), 3 – drop of amplitude

Fig. 14. Udokumentowane złoże gazu: 1 – zmiana polaryzacji w obrębie złoża, 2 – ugięcie czasowe spągu dolomitu głównego (Ca2), 3 – spadek amplitudy

The next modeling was carried out on object “b” which was found on profile A-A’ (Figs 3, 9, 10) and was initially identified as carbonate reef (Barmuta 2010).

Detailed interpretation was performed on Models III, IV and V which were created for this location. Of most interest in object “b” is the double positive reflex that can be seen in the crown part of the barrier buildup (Fig. 10). This kind of effect in the seismic record can be a result of distinctly different rock properties of the ceiling and bottom part of Main Dolomite (Ca2) bed; where the ceiling part would be characterized by higher porosity and/or saturation, while the bottom part would be compact and unsaturated. Such a configuration would produce an additional positive reflex on the boundary between the zones. The first step in this part of the seismic record analysis was the generation of Model III seismic response (Fig. 15) which was developed based on initial interpretation of the barrier on section A-A’ (Fig. 9) (Barmuta 2010). The model assumes uniform wave velocity within Ca2. The generated wave field (Fig. 15) shows a single positive combined reflex from the ceiling of Basal Anhydrite and Main Dolomite (A2/Ca2). The actual recorded wave field (Fig. 10) depicts a second positive reflex below the reflection from the ceiling of theA2/Ca2 beds. This can be a manifestation of a boundary between the porous and the compact saturated dolomite. This suggestion was further tested by modeling the effect of bipartite Main Dolomite (Ca2) on seismic record and evaluation of the minimum thickness of the upper (porous) part of Main Dolomite that could produce the second positive reflex from aphanitic-compacted and micritic-porous dolomite boundary. For this purpose, Model IV (Fig. 16) was created in which a bed of thickness stair-stepping from 30 m to 0 m and a lower velocity, corresponding to porous and/or saturated dolomite, was inserted into a 50m thick layer of compacted Main Dolomite (Ca2spg) characterized by a 6500 m/s wave velocity.

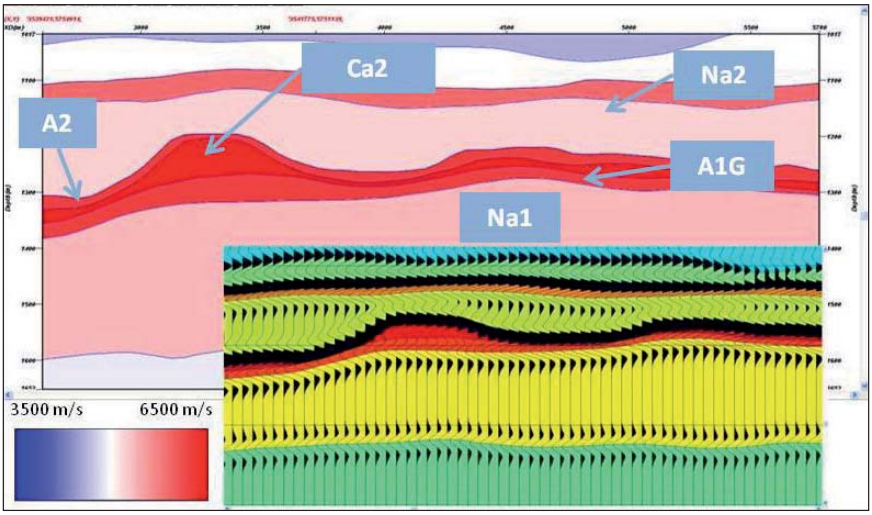

Fig. 15. Model III and its seismic response: Na2 – Oldest Halite, A2 – Basal Anhydrite, Ca2 – Main Dolomite, A1G – Upper Anhydrite, Na1 – Oldest Halite

Fig. 15. Model III wraz z odpowiedzią sejsmiczną: Na2 – sól starsza, A2 – anhydryt podstawowy, Ca2 – dolomit główny, A1G – anhydryt górny, Na1 – sól najstarsza

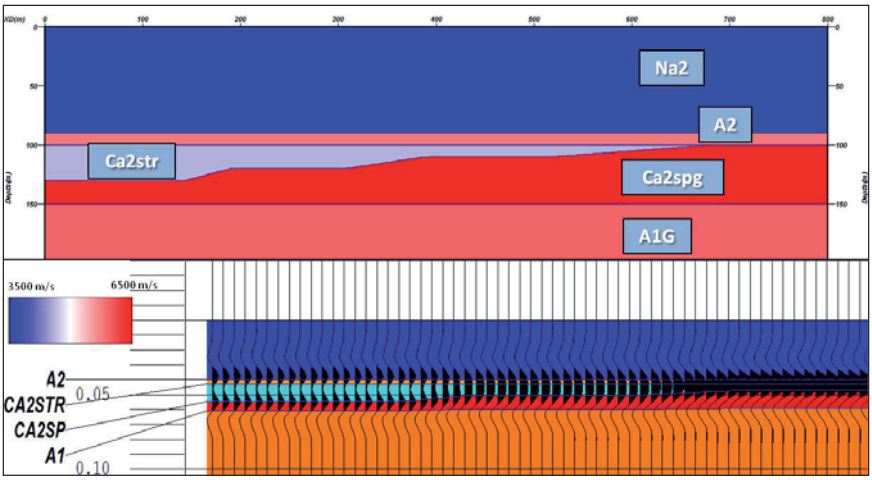

Fig. 16. Model IV which demonstrates the effect of thickness of saturated Main Dolomite layer on seismic response: Na2 – Oldest Halite, A2 – Basal Anhydrite, Ca2str – Main Dolomite (ceiling part, saturated), Ca2spg – Main Dolomite (bottom part, unsaturated), A1G – Upper Anhydrite, Na1 – Oldest Halite

Fig. 16. Model IV przedstawiający wpływ grubości warstwy nasyconego dolomitu głównego na zapis sejsmiczny: Na2 – sól starsza, A2 – anhydryt podstawowy, Ca2str – dolomit główny „stropowy" nasycony, Ca2spg – dolomit główny „spągowy" nienasycony, A1G – anhydryt górny, Na1 – sól najstarsza

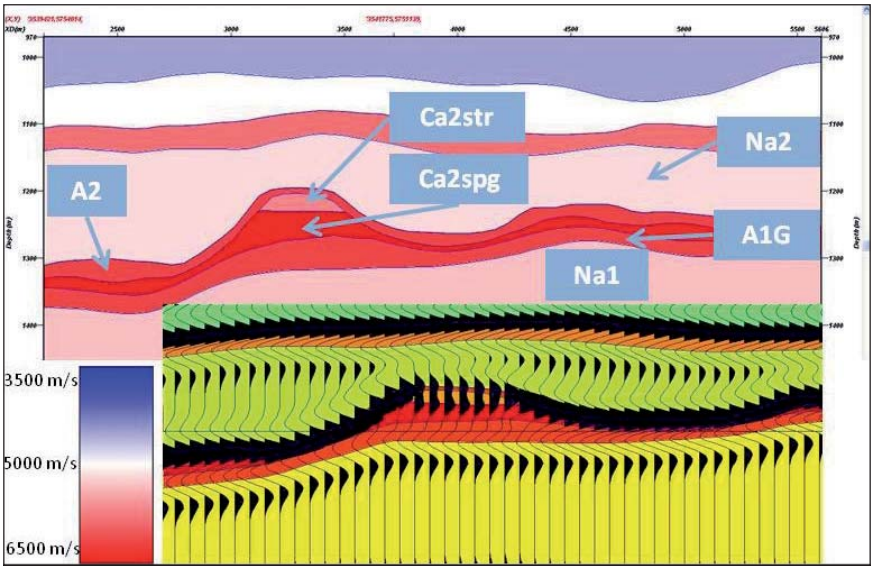

Fig. 17. Model V with generated seismic response: Na2 – Oldest Halite, A2 – Basal Anhydrite, Ca2str – Main Dolomite (ceiling part, saturated), Ca2spg – Main Dolomite (bottom part, unsaturated), A1G – Upper Anhydrite, Na1 – Oldest Halite

Fig. 17. Model V wraz z odpowiedzią sejsmiczną: Na2 – sól starsza, A2 – anhydryt podstawowy, Ca2str – dolomit główny „stropowy" nasycony, Ca2spg – dolomit główny „spągowy" nienasycony, A1G – anhydryt górny, Na1 – sól najstarsza

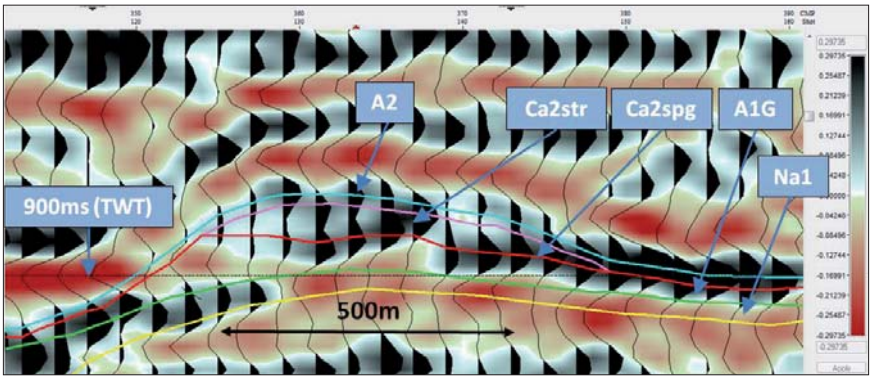

Fig. 18. Reinterpretation of reef barrier based on established models: Na2 – Older Halite, A2 – Basal Anhydrite, Ca2str – Main Dolomite (ceiling part, saturated), Ca2spg – Main Dolomite (bottom part, unsaturated), A1G – Upper Anhydrite, Na1 – Oldest Halite

Fig. 18. Reinterpretacja bariery rafowej na podstawie przeprowadzonych modelowań: Na2 – sól starsza, A2 – anhydryt podstawowy, Ca2str – dolomit główny „stropowy" nasycony, Ca2spg – dolomit główny „spągowy" nienasycony, A1G – anhydryt górny, Na1 – sól najstarsza

This virtual layer (Ca2str) was assigned a wave velocity of 5200 m/s as is typically recorded in boreholes for porous and saturated dolomite. In Model IV, the bed above is 10 m thick Basal Anhydrite which is assigned a wave velocity of 6000 m/s. The upper half-space consists of Older Halite with a wave velocity of 4500 m/s. The bed underlying Main Dolomite is Upper Anhydrite (A1G) of 6500 m/s wave velocity. The generated seismic response from the model (Fig. 16) constructed in this way shows a discernible positive reflex from the boundary between compact and porous dolomite at the location where the porous bed reaches 30 m thickness (Ca2spg – Fig. 16). This observation was further used to modify the earlier interpreted barrier by splitting Main Dolomite with a horizontal boundary, creating in this way a 30 m thick bed having a 5200 m/s wave velocity (Fig. 17 – Model V). The seismic response from the altered model shows a good match with actual seismic records (Figs 9, 10) This allows, in accordance with the assumptions, for a conclusion regarding the bipartite character of Main Dolomite. Based on the results obtained it can also be inferred that the crown part of the reef at object "b' (Fig. 18), characterized by lower velocity, can be a zone of increased porosity and saturation.

CONCLUSIONS AND DISCUSSION

The objective of the research was to demonstrate the applicability of seismic modeling in the structural and prospective interpretation of objects having a size close to the seismic resolution, under conditions of poor quality seismic data, scarce geophysical borehole logs and insufficient geological information.

The subject of the analysis was the data obtained from seismic survey 2D Nowa Sól – Wschowa project carried out by Geofizyka Toruń in 1982–1984 as well as borehole geophysics data obtained in the nineteen-sixties and seventies. The geophysical survey was designed to investigate the development of Main Dolomite Ca2 and to identify gas reservoirs. The poor quality of the seismic data and scarcity of geophysical velocity logging in the boreholes make it difficult to perform a reliable interpretation. Seismic modeling becomes a supporting tool in this situation.

The results of modeling within the research area, on the seismic profiles of cyclothems Werra and Stassfurt of Zechstain formation show:

- the deep sea zone is indicated by positive reflection from the Basal Anhydrite A2 ceiling and negative reflection at the Oldest Halite Na1 ceiling;
- small reservoir zones (velocity drop related to the increase of porosity and/or saturation) are characterized by a change to negative of the reflection at A2 (bright spot type), and time sag at the bottom of Ca2 (typical DHI indicators);
- vertical zonal structure of Main Dolomite (Ca2) of which the upper part is porous and/or saturated (low wave velocity) while the lower part – compact dolomite – manifested by the additional positive reflex on the boundary between the two zones.

The seismic signatures based on modeling allow for the recognition of object "a" and object "b", identified on seismic profile A-A' (Figs 9, 10), as zones of higher porosity and saturation. This statement is confirmed by seismic image of a well-documented reservoir (Fig. 14).

Unfortunately, the number of factors influencing final seismic record makes the result of the interpretation uncertain. The lack of necessary borehole logs forced the authors to choose model parameters (e.g. velocity, etc) empirically or to extrapolate them from distant wells. The reliability of the interpretation may also be influenced by the low quality of the seismic data which made phase correlation difficult to perform correctly. It should be understood that similar anomalies within seismic record could be caused by several different factors; e.g. the amplitude drop can be caused by layer thickness changes similar variations in porosity or saturation (Pietsch & Tatarata 2005).

To summarize, it has to be concluded that seismic modeling can be a supporting tool during interpretation, especially in the case of low quality seismic data, a lack of borehole logs and a lack of geological information.

The authors would like to thank San Leon Energy Poland for providing the seismic and borehole data and giving permission for their use.

REFERENCES

Barmuta J., 2010. *Charakterystyka sejsmiczna utworów cechsztyńskich basenu permskiego rejonie złoża Kisielin (zdjęcie Nowa Sól – Wschowa)*. Biblioteka Wydziału Geologii, Geofizyki i Ochrony Środowiska AGH (unpublished).

Dokumentacja otworowa, 1966–1981. Centralne Archiwum Geologiczne, Państwowy Instytut Geologiczny, Warszawa.

Jędrzejowska-Tyczkowska H., Jałowiecki B. & Misiarz P., 1997. Multi parameter seismic signature of reef-like objects within the permian carbonate deposits. *59th EAGE Conference and Technical Exhibition, Geneva, 1997. Extended Abstracts, 1, PO162. Poster*.

Karnkowski P.H., 2007a. Petroleum Provinces in Poland. *Przegląd Geologiczny*, 55, 12/1, 1061–1067.

Karnkowski P.H., 2007b. Permian Basin as a main exploration target in Poland. *Przegląd Geologiczny*, 55, 12/1, 1003–1015.

Kotarba M.J. (red.), 2009. *System naftowy i ocena zasobów prognostycznych utworów dolomitu głównego w południowo-zachodniej części monokliny przedsudeckiej* (raport z realizacji grantu MNiSW). Archiwum KAŚiGG, Wydz. GGiOŚ AGH.

Niedbalec S. & Radecki S., 2007. Hydrocarbon Accumulation in Poland. *Przegląd Geologiczny*, 55, 12/1, 985–991.

Pietsch K. & Tatarata A., 2005. Próba wykorzystania analiz amplitudowych zapisu sejsmicznego do określenia własności zbiorowiskowych dolomitu głównego. *Geologia* (AGH-UST quarterly), 31, 3–4, 275–296.

Pikulski L., 1996. Analiza paleostrukturalna utworów dolomitu głównego w rejonie bloku Gorzowa. *Nafta-Gaz*, 8, 325–334.

Pikulski L. & Protas A., 1997. Warunki sedymentacji oraz rozwój litofacjalny utworów dolomitu głównego w rejonie bloku Gorzowa. *Nafta i Gaz*, 9, 400–406.

Stupnicka E., 1997. *Geologia regionalna Polski*. Wyd. UW, Warszawa.

Sztormwasser E., 1999. *Objaśnienia do szczegółowej mapy geologicznej Polski 1:50 000. Arkusz Nowa Sól (G12)*. Państwowy Instytut Geologiczny, Warszawa.

Urbański K., 1998. *Objaśnienia do szczegółowej mapy geologicznej Polski 1:50 000. Arkusz Zielona Góra (526)*. Państwowy Instytut Geologiczny, Warszawa.

Wagner M.R., 1994. Stratygrafia osadów i rozwój basenu cechsztyńskiego na Niżu Polskim. *Prace PIG*, 146, 1–71.

Widess M.B., 1973. How thin is a thin bed. *Geophysics*, 38, 6, 1176–1180.